Astron. Astrophys. 319, 673–682 (1997)

ASTRONOMY
AND
ASTROPHYSICS

Cycle 19 facula dynamics

I. Angular rotation

N. Meunier[1], **E. Nesme-Ribes**[1], **and N. Grosso**[1]

URA 2080 CNRS, Département d'Astronomie Solaire et Planétaire, Observatoire de Paris, 5 Place Janssen, F-92195 Meudon, France

Received 20 May 1996 / Accepted 14 August 1996

Abstract. Our analysis of photospheric facula rotation throughout cycle 19 has yielded a number of new findings: (1) The existence of a strong north-south asymmetry of the rotation rates (of as much as 1 °/day), related to the magnetic activity level. (2) The presence of two distinct populations that possibly reflect the complexity of dynamo waves at the interface between the convective zone and the radiative zone. (3) A pattern of slow/fast rotation zones similar to the magnetic torsional oscillation discovered by Snodgrass (1991). Facula rotation showed little time-dependence throughout solar cycle.

Key words: Sun: faculae – Sun: rotation – Sun: activity – Sun: magnetic fields – sunspots

1. Introduction

The coupling between solar magnetic fields and convective flows is of importance for modeling the solar nonlinear dynamo, in which the back-reaction of magnetic fields on flows must be taken into account (for a review, see Roberts 1994). Among the questions to be addressed, the dynamics of the various magnetic scales is of crucial importance. Sunspots have been widely used, and notably to probe the deep convective layers (Collin et al. 1995). Photospheric faculae are also the manifestation of concentrated azimuthal fields. They are more widely distributed than sunspots, and persist longer. However, magnetic fields within a facula might be less intense than in sunspots, and thereby the coupling with surrounding plasma would be different.

There is a need for extensive study of facula rotation. Attempts have been made to track individual faculae (by following their barycenter motion) by Belvedere et al. (1977). These authors found that smaller faculae rotate faster than larger ones, whatever the compactness. Their study is subject to rather large uncertainties: the barycenter of a facula is determined with an error of about 10% in the $\pm 25°$ latitude belt. Magnetic elements visible on the Kitt Peak magnetograms can also be used to determine solar rotation, and there is a close correspondence between these features and photospheric faculae (Nesme-Ribes et al. 1996a). Komm et al. (1993) studied the rotation of magnetic elements through cycle 21, with much better precision than Belvedere et al. (1977), and obtained a rotation distribution close to that of the unmagnetized convective layers. Komm et al. also observed some variability in the differential rotation through the solar cycle as shown by cycle 21 sunspots, but of smaller amplitude. Antonucci et al. (1990) performed a Fourier analysis of large-scale photospheric features on magnetograms, by latitude bands, and detected a strong north-south asymmetry of the rotation rate (a north-south difference larger than 0.5°/day at mid-latitudes) for the first time at the photospheric level.

The aim of this paper is to make an extensive analysis of the rotation of photospheric facular bright points during cycle 19. In a companion paper (Meunier et al. 1996, referred to hereafter as Paper II), we shall present results concerning meridional circulation and Reynolds stresses that are of fundamental importance for the maintenance of the differential rotation in the convective zone. We first present the data and the tracking procedure (Sect. 2), and then discuss a possible bias inherent in spectroheliograms, in Sect. 3. The north-south asymmetry throughout cycle 19 is examined in Sect. 4. The time-dependence of the facula rotation rate is discussed in Sect. 5. Our data reveal the existence of two distinct populations, whose characteristics are listed in Sect. 6. Lastly, a torsional oscillation pattern is traced by faculae (Sect. 7).

2. Observational data and tracking procedure

Our study deals with faculae displayed on the Meudon K_{1v} spectroheliograms (1.5 Å off the Ca II K line center with a 0.14 Å passband), which show faculae and sunspots at the photospheric level. The height of formation of K_{1v} is approximately 500 km (Vernazza et al. 1981). This is close to the height of about 425 km for a 1000-gauss field and of 300 km for a 2000-gauss field above the $\tau = 1$ level, which are commonly used values (Nesme-Ribes et al. 1996a).

Send offprint requests to: N. Meunier

K_{1v} spectroheliograms have been digitized with 1.8 arcsec pixel size, which is the average spatial resolution obtained at Meudon. The solar radius is determined as follows. An approximated limb is first detected with a fixed brightness threshold. Then an inflection point is found by interpolating the radial intensity profile at each point of the approximated limb, yealding a better definition of the limb. Inherent scanning distortions are corrected (Mein & Ribes 1990) using the resulting radius versus polar angle: spectroheliograms are selected whose radius dispersion is less than one pixel.

The procedure for tracking the bright points forming a facula was described in Collin et al. (1995). We visually associate if possible each facular point present in a given image with the point corresponding to it in the following image. From this, we get the rotation rate and meridional motion for each facular point. Each bright point selected has an average size of 2 to 6 arcseconds. The number of points selected within a given facula depends on the facula size, its compactness, and the seeing conditions. This differs from studies in which the rotation is determined by the displacement of the faculae barycenter (Belvedere et al. 1977). In practice, our selection applies to well-defined faculae, or parts of faculae only, and discards the rest. The rotation rate corresponding to a given facula contains an additional component due to the time variation of the facula. We could identify about 160 points per image pair without ambiguity when the Sun was active. As we restricted our study to high-quality images, an average of 66 pairs were selected each year. A total of 47434 points were tracked over the period 1957-1964.

3. Sources of error

In earlier papers (Mein & Ribes 1990; Collin et al. 1995), we listed the various errors inherent in spectroheliograms and in the tracking procedure used. The random error on each velocity measurement is 15 m/s at the disk center. But there is one cause of distortion that has been largely overlooked: the curvature of spectral lines after passing through the dispersing system. It is well-known that prisms and gratings curve the spectral lines. This can theoretically be corrected with a judicious choice of spectrograph exit slit. Before 1989, the Meudon spectroheliograph was equipped with two dispersing systems: a grating for the H_α line and prisms for the Ca II K line. Each system introduced a different curvature for each line. For reasons of convenience, a single exit slit was adopted at that time, and its curvature was a compromise for the two lines (Ca II K and H_α). As a result, a second order curvature effect remains in the K_{1v} spectroheliograms, leading to an east-west asymmetry that we detected. However, we cannot exclude other unknown causes for east-west asymmetry. If the bright points were uniformly distributed over the solar disk, there would be as many east points as west, so the averaged rotation would not show any significant bias. However, the distribution is not homogeneous so the bias has to be corrected.

The slit bias is corrected as follows. We first compute the latitude-averaged rotation rate versus disk longitude, referred to as the "observed bias". Then we calculate the bias we would observe with the real point distribution on the disk, but with the longitude-averaged observed rotation rate (i.e. with latitude-dependence only). Then we subtract this synthetic bias from the observed one, which gives the "real bias" shown in Fig. 1. This is necessary to take the north-south distribution of points into account along with the differential rotation. A linear fit over the whole cycle has a slope of -2.075 10^{-3} day^{-1}. This mean bias reaches one pixel, and shows a linear longitude-dependence over the [-50°,40°] range. This curve does not seem to vary much with the cycle phase, and is latitude-independent. Because there are few sunspots compared with facular elements, the bias was smoothed out by the large dispersion of rotation rates in previous sunspot studies of the same images.

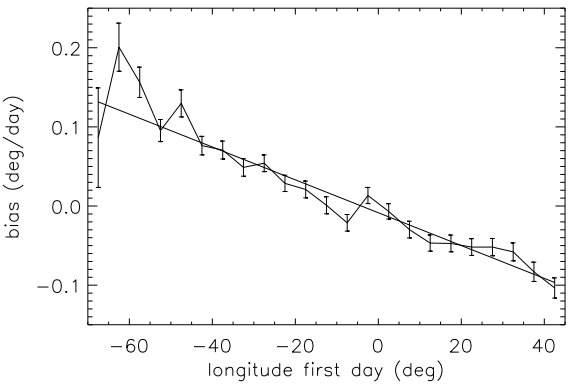

Fig. 1. "Real bias" in degrees/day versus the facular points longitude of the first day of the image pair. This bias is obtained by subtracting a synthetic bias (rotation versus longitude for the real point distribution and an average rotation with a latitude-dependence only) from the observed rotation versus longitude. The straight line is a linear fit on the curve, and has a slope of -2.075 10^{-3} day^{-1}

Assuming the bias to be negligible at the disk center, the rotation rate can be corrected for each longitude and for the whole data set. The bias (Fig. 1) is linearly modeled as

$$bias = ax + b, \tag{1}$$

where x is the disk longitude, and a the slope (-2.075 10^{-3} day^{-1} as determined from Fig. 1). Then the correction to be applied to longitude-averaged rotation rates is

$$Corr = \left(\frac{\sum_{i=1}^{N} N_i x_i}{\sum_{i=1}^{N} N_i} - \frac{\sum_{i=1}^{N} x_i}{N} \right) a, \tag{2}$$

where x_i is the longitude of a bin, N_i the number of points within the bin, and N is the number of bins. Table 1 lists the corrections applied to faculae for the different years. In the following sections, facula rotation rates will be corrected using Table 1.

4. Rotation of photospheric faculae: north-south asymmetry

Facular angular rotation is given in sidereal rates. We show angular sidereal rates for facular bright points (Fig. 2) after

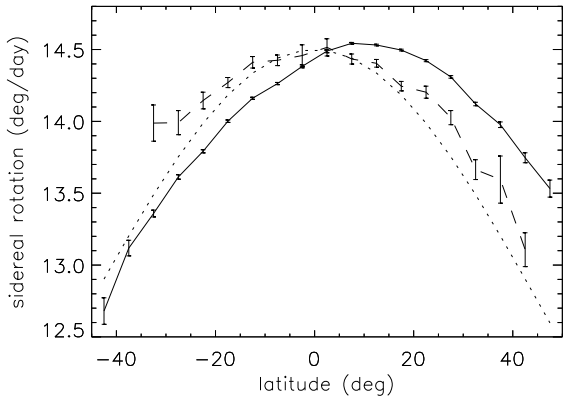

Fig. 2. Faculae sidereal rotation rate from 1957 to 1964 (solid line), after correction of the slit bias, and sunspots rotation from 1957 to 1962 (dashed line). Values are given in degrees/day. The error bars are at the 1-σ confidence level and are very small for faculae (smaller than 0.01°/day for most of the latitude bins)

Table 1. Corrections in degrees/day for each period

year	$Corr$
1957	-0.008
1958	-0.010
1959	-0.019
1960	-0.016
1961	-0.018
1962	-0.021
1963	-0.017
1964	-0.018
1957-1960	-0.020
1961-1964	-0.018
1957-1964	-0.021

correction. Mean rates have been calculated for 5° latitude bins, for each year of the interval 1957 to 1964. The error bars are the standard 1-σ errors δ_i on the mean. The corrections showed in Table 1 are of the order of 1-σ errors in the rotation rates of Fig. 2, which justifies the need for corrections. But we shall see that the correction factor is smaller than the error on the first coefficient of the polynomial fit. Therefore it is a zero-order correction that does not significantly alter the results presented in this paper.

The main result is a strong asymmetry with respect to the equator. At a latitude of 30°, the northern hemisphere rotates about 1°/day faster than the southern. This north-south asymmetry persists throughout cycle 19 and was also visible in 1982 (Collin et al. 1995) and during cycle 21 (Antonucci et al. 1990), though the amplitude was smaller. It is interesting to note that the more active the hemisphere, the more rigid-like it rotates, and the faster. So we deduce from this asymmetry that the magnetic field rotates more rigidly than the unmagnetized convective layers (Nesme-Ribes et al. 1993; Collin et al. 1995).

4.1. Age-dependence of facula rotation

We sorted faculae by age. In some latitude bands, young faculae (4 days old or less) rotate slightly faster than the much more numerous older ones (92.5 % of the whole data set). But this effect is not detected in all the latitude bands and is of small amplitude (about 0.1°/day). So we found no systematic difference due to facular age. Belvedere et al. (1977) reported a significant difference of some 3.5% between small facula rotation rates and those of larger ones. Ternullo (1986), using the same data set than Belvedere et al., reported a significantly slower and more rigid rotation of old faculae, and thus confirmed the age-dependence of facula rotation found by Belvedere et al. This difference is not present in our data.

4.2. Comparison with cycle 19 sunspots

Sunspot rotation has also been studied within a similar time interval [1957-1962] (Nesme-Ribes et al 1996b). Surprisingly, sunspot rotation shows no significant north-south asymmetry, at least in the [-30°,30°] latitude range (Fig. 2).

4.3. Comparison with magnetic photospheric elements

Bright magnetic features visible on Kitt Peak magnetograms have almost a one-to-one correspondence with K_{1v} faculae (Nesme-Ribes et al. 1996b). Komm et al. (1993) analyzed magnetic element motion for cycle 21. Their tracking procedure is a 2-D cross-correlation of brightness. They found no pronounced north-south asymmetry, in contrast with K_{1v} faculae of the same period (see Fig. 3 of Komm et al. 1993, and Fig. 1 of Collin et al. 1995) or with Antonucci et al. (1990) Fourier analysis of Mount Wilcox magnetograms. A preliminary comparative study of the various tracking procedures shows that north-south asymmetry is smoothed out by a 2-D cross-correlation technique. This point deserves further study. We also suspect that the tracking procedure adopted by Komm et al. favors the selection of lingering magnetic elements; but this does not explain the fact that these authors do not observe any strong north-south asymmetry.

5. Time-dependence of faculae rotation throughout cycle 19

It is convenient to characterize solar rotation and its variability through the cycle with a polynomial fit. We recall that facular rotation rates are corrected for the bias discussed in Sect. 3. We use orthogonal Legendre polynomials with odd and even coefficients because of the strong north-south asymmetry. For the same reason, nothing is gained by folding the two hemispheres. The data set consists of mean angular rotation rates (Ω_i) calculated for 5° latitude bins. The Ω_i values are weighted by the number of points within each bin. The Legendre coefficients are obtained using a least-squares minimization, and are then converted into the widely used coefficients A_j, such that the rotation rate $\Omega(\theta)$ is represented by

$$\Omega(\theta) = \sum_{j=0}^{4} A_j \sin^j \theta. \quad (3)$$

Table 2. Coefficients of the expansion $\Omega(\theta) = \sum_{j=0}^{4} A_j \sin^j \theta$ (θ the latitude) for cycle 19 faculae sidereal rotation rate in degrees/day. Errors are obtained with the Monte Carlo simulation and are at the 1-σ confidence level

year	A_0	σ_0	A_1	σ_1	A_2	σ_2
1957	14.467	0.077	0.859	0.194	-2.43	1.04
1958	14.463	0.036	0.920	0.136	-2.16	0.55
1959	14.468	0.031	0.993	0.137	-2.62	0.48
1960	14.423	0.036	0.892	0.182	-2.40	0.83
1961	14.390	0.037	0.905	0.232	-1.76	1.21
1962	14.425	0.060	1.070	0.307	-2.66	1.76
1963	14.359	0.100	0.952	0.381	-2.43	2.87
1964	14.438	0.052	1.082	0.308	-3.30	1.08
1957-1964	14.424	0.017	0.906	0.069	-2.17	0.29
1957-1960	14.463	0.020	0.907	0.078	-2.30	0.33
1961-1964	14.419	0.030	0.941	0.161	-2.22	0.80

year	A_3	σ_3	A_4	σ_4
1957	-0.18	0.81	-0.37	2.71
1958	-0.66	0.73	-0.62	1.61
1959	-1.01	0.82	0.39	1.65
1960	-1.16	1.25	0.28	2.88
1961	-0.42	2.34	-1.95	7.07
1962	-2.49	1.99	2.19	6.66
1963	-1.80	4.47	5.36	17.13
1964	-1.11	1.94	-2.01	3.88
1957-1964	-0.63	0.40	-0.71	0.86
1957-1960	-0.61	0.42	-0.51	0.91
1961-1964	-0.82	1.33	-0.71	3.20

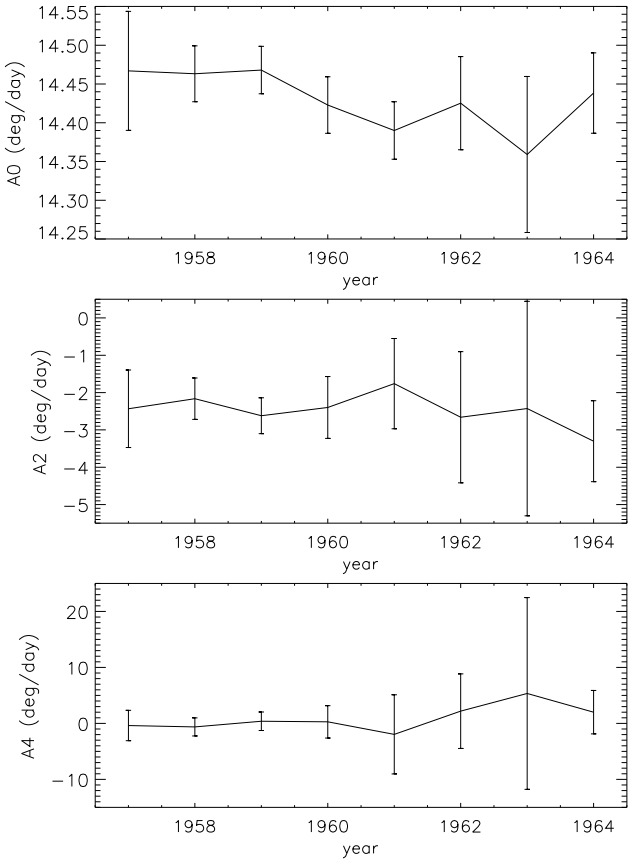

Fig. 3. Variation of the even coefficients of the expansion $\Omega(\theta) = \sum_{j=0}^{4} A_j \sin^j \theta$ (θ the latitude) for cycle 19 faculae sidereal rotation rate. From top to bottom: A_0, A_2, and A_4. Errors are at the 1-σ confidence level

We adopted a fourth-degree polynomial expansion, because a second-degree expansion offers a poor fit of the data, and a sixth-degree polynomial expansion or higher is not necessary, since the number of points at high latitudes is small.

We also compute the errors σ_j on the A_j coefficients. Errors on Legendre coefficients are often calculated as $\sqrt{C_{jj}}$, where C is the estimated covariance matrix (weighted by δ_i) of the fitted points. To check these, we perform a Monte Carlo simulation with a thousand trials (Press et al. 1986), in which the dispersion of the coefficients gives 1-σ error on A_j. The errors obtained by the Monte Carlo method are then smaller for the first coefficients but higher for the later ones. We consider only errors determined by this method.

5.1. Phase-dependence of facular rotation

Expansion (3) coefficients for faculae and corresponding errors computed with the Monte Carlo method are listed in Table 2. A_0 represents the equatorial rate, A_2 and A_4 the rotation at low and high latitudes respectively, and A_1 and A_3 characterize the north-south asymmetry at low and high latitudes.

Figures 3 and 4 show the variability of the facular rotation rate throughout cycle 19. Let us note that the cycle maximum occurred in 1958 and 1959, and the minimum in 1963. In 1964, we begin to see some activity of cycle 20 starting at high latitudes. The main significant variation is the decrease of A_0 from the cycle maximum to the minimum by about 0.4%. Comparing the two periods [1957-1960] (strong activity) and [1961-1964] (low activity), a difference of some 0.05°/day can be seen between the active and quiet periods. A_2 and A_4 variations are hardly significant; but we observe that A_2 tends to decrease (which means a more differential rotation at cycle minimum). We also compute the correlation factor between the expansion coefficients obtained from the Monte Carlo simulations, which yields similar values. The coefficients are not completely independent, and the observed variations of A_2 and A_4 are not significant.

A_1 and especially A_3 variations, representing the north-south asymmetry, at low and high latitudes respectively, are hardly significant. The antisymmetric part of the rotation rate, $A_1 \sin\theta + A_3 \sin^3\theta$, for the periods [1957-1960] and [1961-1964] for $|\theta| < 25°$, is very similar. The amplitude is only slightly smaller for the period [1961-1964] at high latitudes ($|\theta| > 40°$). Our preliminary conclusion is that we cannot detect any variations of the north-south asymmetry through cycle 19.

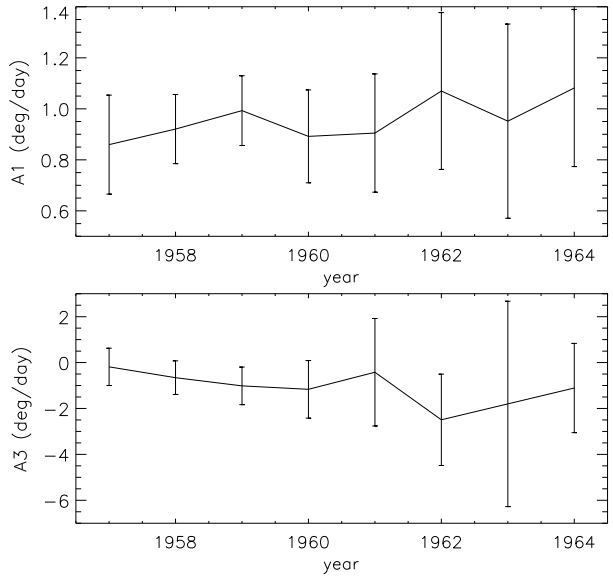

Fig. 4. Variation of the odd coefficients of the expansion $\Omega(\theta) = \sum_{j=0}^{4} A_j \sin^j \theta$ (θ the latitude) for cycle 19 faculae sidereal rotation rate. Top: A_1 and bottom: A_3. Errors are at the 1-σ confidence level

Table 3. Coefficients of the expansion $\Omega(\theta) = \sum_{j=0}^{4} A_j \sin^j \theta$ (θ the latitude) for cycle 19 sunspot sidereal rotation rate in degrees/day. Errors are obtained by Monte Carlo simulation, and are at the 1-σ confidence level

year	A_0	σ_0	A_1	σ_1	A_2	σ_2
1957-1962	14.473	0.062	0.086	0.238	-1.89	0.99

year	A_3	σ_3	A_4	σ_4
1957-1962	-0.71	1.52	-1.47	3.51

5.2. Comparison with sunspots

We compared these results with sunspot rotation rates obtained for the period [1957-1962] (Table 3). We shall recall that sunspot data have not been corrected for the bias mentioned in Sect. 3, because the small number of sunspots yields to large errors compared to the correction. Sunspot rotation exhibits no significant north-south asymmetry, and is also more rigid (see A_2) than that of faculae, which is consistent with a deeper anchorage of intense magnetic fields (Collin et al. 1995).

6. First detection of another asymmetry

As shown in Fig. 5, rotation rates exhibit a large dispersion about the mean. The rms velocity is 3% of the mean rotation rate, and certain facular points show a deviation of more than 7% from the mean rotation rate. There are a number of reasons of instrumental and solar origin for the dispersion in the angular velocity. Instrumental errors have been discussed in Sect. 3. To address the solar causes, we subtracted the mean differential rotation (i.e. the Legendre polynomial fit) from each individual rotation rate. Then we plotted the corresponding histogram

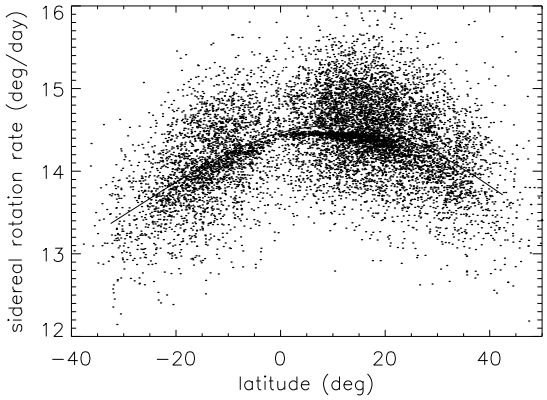

Fig. 5. Selected facular points in 1959, and polynomial fit of the average rotation (Sect. 5)

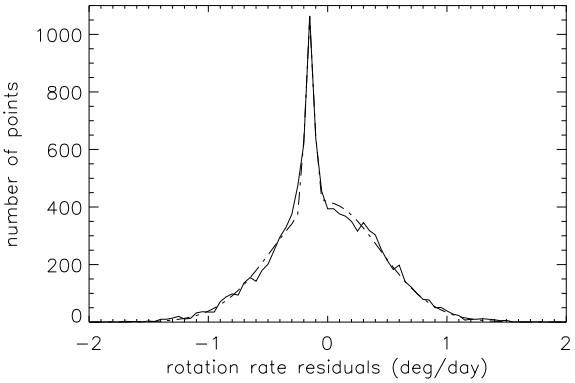

Fig. 6. Histogram for 1959 faculae (solid line) with a 0.05°/day bin, a two-gaussian fit has been applied to the data (dashed line)

distribution in 0.05°/day bins (Fig. 6). One striking result is the existence of a sharp peak in an otherwise roughly gaussian distribution (this phenomenon will be referred to hereafter as a shape-asymmetry). The histogram seems to indicate the existence of two populations: one (denoted hereafter population I) exhibiting rotation close to the mean, and another (population II) that rotates slower than average, with much smaller dispersion. As it may seem difficult at first sight to separate population II from population I, we shall attempt to identify the properties of each.

6.1. Histogram asymmetry

In a first step, we define a parameter r representing the proportion of points below and above the mean as

$$r = \frac{L - R}{T}, \tag{4}$$

where R and L are the number of facular points having a rotation rate higher and lower, respectively, than the fit of Fig. 6, and T is the total number of points. r is of particular interest because the whole population II rotates slower than the average. Considering

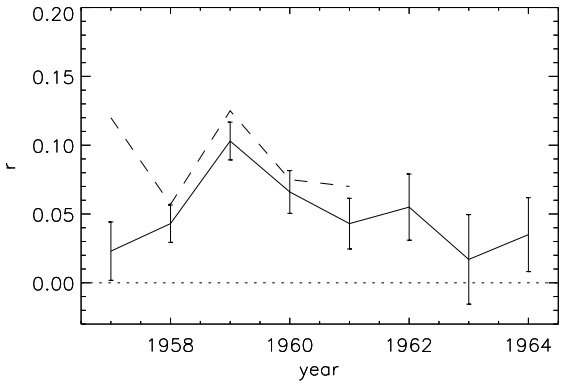

Fig. 7. Variation of the ratio r for faculae (solid lines) between 1957 and 1964 and for sunspots (dashed line) between 1957 and 1961. Error bars are not shown for sunspots to make the graph easier to read: they are slightly smaller than the r values

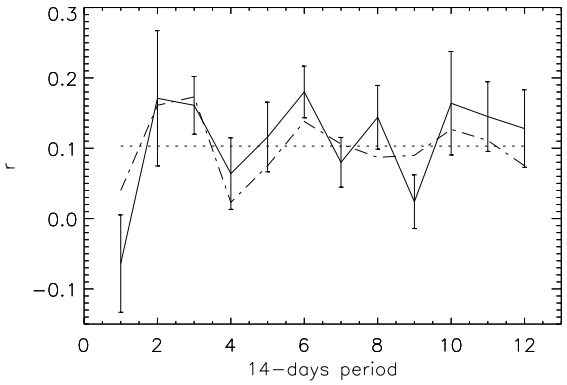

Fig. 8. Variation of r for faculae versus 14-day period number in 1959, using the yearly fit (solid line) and the 14-day period fit (dashed line). Error bars are shown for only one curve, to make the graph easier to read; however, they do not differ from one curve to the other

Table 4. Shape-asymmetry parameter r for faculae during [1957-1964]

selection	r
all	0.058 ± 0.010
young	0.082 ± 0.025
old	0.057 ± 0.011

the uncertainty on a number of points N to be $\sqrt{N}$, and assuming that r is small ($L \sim R \sim T/2$), the error on r is given by

$$\sigma_r = \frac{\sqrt{L}}{T} + \frac{\sqrt{R}}{T} + \frac{|L-R|}{T\sqrt{T}} \sim \sqrt{\frac{2}{T}}. \quad (5)$$

The variation of r over the period [1957-1964] is given in Fig. 7. r is maximum at sunspot maximum. As shown in Table 4, no significant difference is found in the shape-asymmetry of young and old faculae.

We also checked to see whether the shape-asymmetry is time dependent. For this purpose, we grouped the image pairs in 14-day periods (approximately half a solar rotation). The number of pairs in each period is of course not constant, because of observation gaps. Then we compute the shape-asymmetry r of the rotation rate histogram in two ways: by subtracting from the individual rotation rates (1) the polynomial fit of the corresponding 14-day period; or (2) the corresponding yearly polynomial fit. The latter means that points of the histogram are at the same position as those for the yearly histogram: zero is the same. The results are very similar, as shown in Fig. 8 for 1959. r oscillates with a period about 1.5 solar rotations throughout the year. The oscillation amplitude is hardly greater than the noise; however, if such an oscillation persisted throughout the cycle, it would hint at the existence of giant cells. This deserves further study.

6.2. Activity-dependence of facula shape-asymmetry

The next question to be addressed is whether the two populations differ by their activity level or size. We know that larger sunspots or sunspot groups rotate more slowly than smaller ones (Maunder & Maunder 1905; Newton & Nunn 1951; Ward 1966). One would thus expect that slowly rotating faculae (population II) would correspond to the larger faculae. The parameter r is higher in the northern hemisphere, which suggests a relation with the solar activity level. So we compare the north-south asymmetry of the shape-asymmetry with that of activity. We calculated the two north-south asymmetry parameters, each year, as follows

$$A_s = \frac{\Delta N - \Delta S}{\Delta N + \Delta S}, \quad (6)$$

where ΔN and ΔS are the differences between the number of points below and above the fit, for the northern and southern hemispheres, respectively, and

$$A_a = \frac{N - S}{N + S}, \quad (7)$$

where N and S are the number of active regions weighted by their activity level X, for the northern and southern hemispheres, respectively. X varies from 1 (quiet) to 10 (very active region), and reflects the size of the facula, the number of sunspots, and its lifetime. The errors on A_s and on A_a are, respectively,

$$\sigma_s = \frac{\sqrt{\Delta N} + \sqrt{\Delta S}}{\Delta N + \Delta S}(1 + |A_s|), \quad (8)$$

$$\sigma_a = \frac{\sqrt{N} + \sqrt{S}}{N + S}(1 + |A_a|). \quad (9)$$

We computed A_a for all X, $X = 1$ and $X \geq 5$. Results are shown in Fig. 9. No conclusion is possible as to whether or not the shape-asymmetry is due to very active regions. However the shape-asymmetry is probably related to the activity level.

6.3. Population I and II splitting

Another approach consists in selecting points from population II as follows. We know that population II facular points exhibit

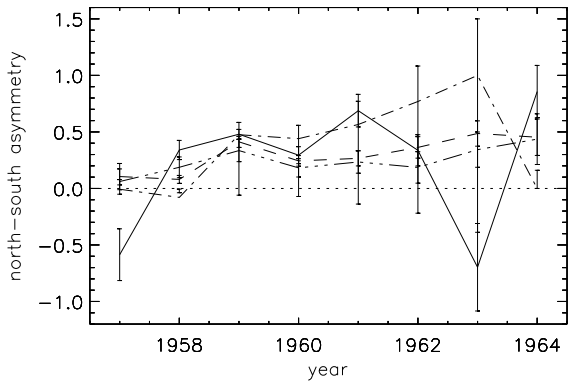

Fig. 9. Variation of A_a for all X (dashed line), $X = 1$ (dot-dot-dot-dashed line), $X \geq 5$ (dot-dashed line), and of A_s (solid line)

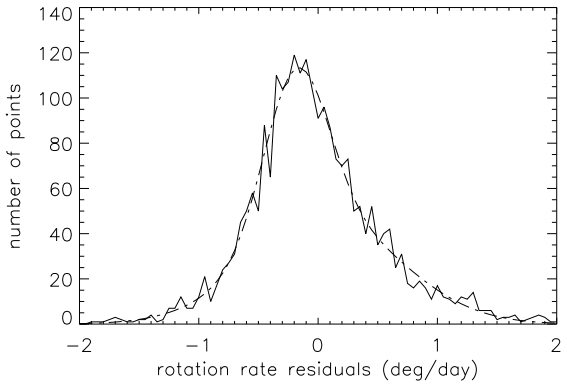

Fig. 10. Sunspots histogram in [1957-1962] (solid line) with a 0.05°/day bin and a two-gaussian fit (dashed line)

small rotation rate dispersion. This is particularly true for the northern hemisphere at low latitudes (see Fig. 5). We investigate the particular case of 1959, for which the shape-asymmetry is the strongest ($r_{1959} = 0.103 \pm 0.014$). We select points corresponding to this concentration within the rotation range $14.25 < \Omega < 14.5$ °/day and the latitude range $0° < \theta < 20°$. This restricted data set still contains points belonging to population I, but we estimate that half the sample belongs to population II (instead of the approximate 10% for the whole set of points). The results are as follows: (i) populations I and II show no significant disk longitude-dependence; (ii) both populations show two preferential longitudes (measured by Carrington longitudes); (iii) the meridional circulation of population II facular points seems negligible, in contrast to that of population I, which is one order of magnitude greater. This point will be investigated in a companion paper (Paper II).

The above procedure is rather arbitrary. However, a two-gaussian fit was also performed in each latitude bin to characterize the rotation rates precisely by two curves associated with two dispersions versus latitude, and this selection showed similar results.

6.4. Comparison with sunspots

Additional information can be obtained from sunspots during the same period. Sunspots also have a shape-asymmetry of the rotation rate distribution (Fig. 10). However, in contrast with faculae, the "peak" is broadened, suggesting that populations I and II are more mixed. The degree of asymmetry r is comparable to that of faculae (Table 5). The sunspot shape-asymmetry seems to be age-dependent, with old sunspots having a larger r than younger ones. But there is no significant difference between leaders and followers, which indicates that the whole active region contains one population or the other. There is no difference either, however complex the group might be.

The comparison between sunspots and faculae is not straightforward. A facula contains many more points than a sunspot group, and its lifetime is longer. Therefore the large peak present in the facular rotation histogram might be due to a limited number of very large and long-lasting faculae.

Table 5. Shape-asymmetry parameter r for sunspots during [1957-1962]

selection	r
all	0.107 ± 0.028
young	0.063 ± 0.051
old	0.319 ± 0.100
leader	0.125 ± 0.096
follower	0.074 ± 0.106
complex	0.115 ± 0.132

The two-gaussian fits mentioned in Sect. 6.3 emphasize the differences between sunspot and facula shape-asymmetries. While the rms velocity of facula population II is one order of magnitude smaller than that of population I, the ratio is only of 2.4 for sunspots. Moreover, the ratio between the number of sunspots belonging to population I and II is close to 1, while it ranges from 8 to 17 for faculae. This fit also quantifies the difference of rotation rate between populations I and II: 0.13°/day for faculae and 0.23°/day for sunspots.

7. Torsional oscillation patterns

A system of alternating high and low-rotation zones migrating toward the equator has first been observed by Howard & La Bonte (1980), using Mount Wilson velocity data. This pattern, referred to as torsional oscillations, is marginally significant, and the velocity amplitude is of the order of 3 m/s. The latitude of greatest activity was found to be associated with the transition zone between high and low rotation rates (maximum shear zones). More recently, Snodgrass (1991) observed a magnetic torsional oscillation pattern of larger amplitude at high latitudes (20 m/s) from Mount Wilson full disk (λ5250.2 FeI) magnetograms. The small amplitude in the $\pm 40°$ latitude belt might be the reason why such a magnetic pattern has never been observed with sunspots, exclusively present within this zone. The magnetic pattern found by Snodgrass is shifted from the veloc-

Table 6. Gamma function (Γ) for fitting faculae sidereal rotation rates of Table 2

year	Gamma
1957	0.077
1958	0.015
1959	0.045
1960	0.002
1961	0.013
1962	0.005
1963	$9\ 10^{-5}$
1964	0.124

ity pattern of Howard & Labonte, and slow zones correspond to latitudes of strong activity. Schüssler (1981) and Yoshimura (1981) proposed that these torsional oscillations were related to the variations of the mean azimuthal Lorentz force through the solar cycle.

We are now investigating whether the Meudon faculae exhibit a torsional oscillation pattern through the solar cycle. For this purpose, we first tried to subtract the Legendre polynomial fit corresponding to the time-interval 1957-1964 from the yearly averaged data in each latitude bin, as done by the authors mentioned previously. The main finding is that we observe no torsional pattern. This is not surprising if we consider the amplitude of the pattern (a few meters per second) compared to the decrease of A_0 ($\sim$10 m/s) through the cycle. Any torsional effects, if real, would be smoothed out. So the usual procedure of subtracting the whole cycle fit yields no pattern with our data.

We then computed the Gamma function (Γ) corresponding to the polynomial fit performed in Sect. 5 (Table 6), which is an indication of the reliability of the fit. A value of Γ=1 indicates an excellent fit, and Γ close to zero reflects a very poor fit. The Γ values we found are in the intermediate range (0.05 to 0.15). There are two possible explanations for this: either the Γ values are low because errors have been underestimated, or the polynomial fit deviates significantly from real data. If the latter is true, we can overcome the difficulty by plotting the difference between the observed yearly-averaged rotation of each latitude bin and the polynomial fit of the corresponding year (Fig. 11). With this new method, we observe some latitudinal bands that rotate faster and others more slowly than average. This pattern of narrow bands (about 10° wide) is significant at the 1-σ level only. The equatorward displacement of this pattern through the solar cycle is hardly significant. Fig. 11 also displays the distribution of the facular points (a "facula butterfly diagram"). In the northern hemisphere, the region of strong activity seems to lie within the band of slow rotation, as observed by Snodgrass (1991). The opposite seems to be true of the southern hemisphere; but since there is less activity, the signal is less significant. So our torsional oscillation pattern does offer some similarities with Snodgrass' magnetic pattern, but the north-south asymmetry present in our data was not observed by this author.

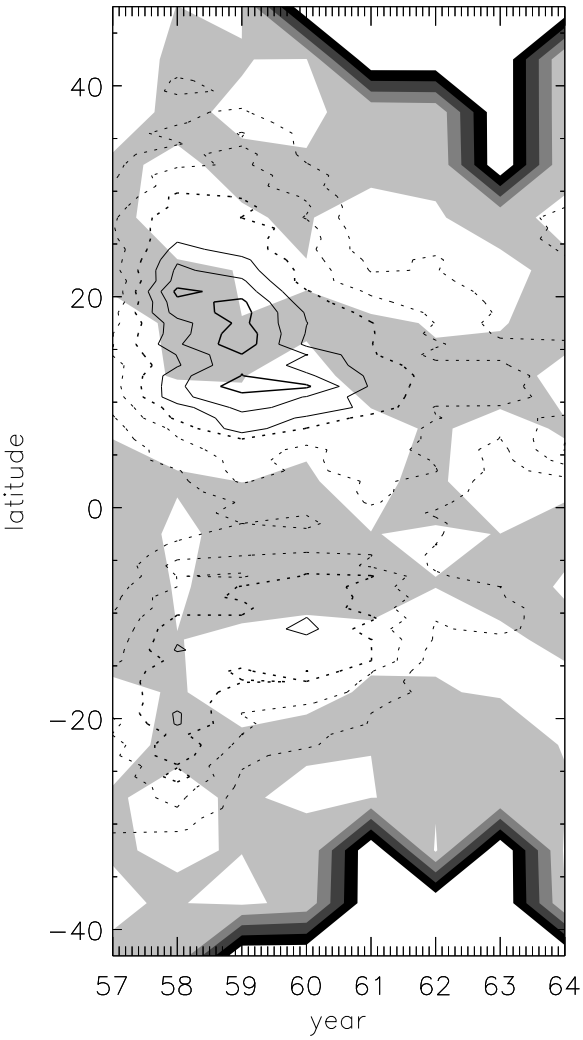

Fig. 11. Torsional oscillation pattern obtained by subtracting the polynomial fit of each year from a yearly averaged values (grey: slower than average, white: rotation faster than average). The amplitude of the pattern is of the order of a few meters per second. The dashed and solid lines represent the "faculae butterfly diagram"

8. Conclusion

Using the Meudon spectroheliograms, we studied photospheric facula angular velocity properties throughout cycle 19. We detected a bias, mainly due to the spectroheliograph slits, which has been corrected.

The main new finding is the detection of two populations of faculae. The facula rms angular velocity distribution is not fully gaussian, but rather presents a strong and narrow peak. This population II (10% of the whole data set) rotates more slowly than the mean (about 1% less), exhibits less meridional circulation, and has a rms velocity ten times smaller than that of population I. This peak is seen mostly for the northern hemisphere in the [0-20°] latitude range and at the cycle maximum (1959). We observe no difference by age, activity level, size, disk longitude or Carrington longitude, and the peak is present during

the whole period. Sunspots show a similar shape-asymmetry, though with different characteristics: the two populations have similar rms velocities and number of points. So sunspot and facula shape-asymmetries may be of different origin.

The shape-asymmetry is maximum at sunspot maximum and is stronger in the northern hemisphere (which rotates faster and more rigidly, and which is also the most active). So the shape-asymmetry may be due to the behavior of the dynamo wave: for example, fluctuations in the dynamo (despite the long lifetime of our shape-asymmetry), as discussed by Hoyng (1993), may be involved. The question is still open. The facula shape-asymmetry is probably related to some surface phenomena. We also note that, because the rotation rate distribution is far from a gaussian, the computed standard errors must be considered with caution.

The second essential finding is the strong, and persistent north-south asymmetry. We did not observe this for sunspots of the same period. This north-south asymmetry imposes constraints on dynamo action, surface velocities, and the transfers between the two hemispheres. In particular, the constant north-south asymmetry observed over the eight years of our data set shows that this phenomenon is not stochastic, since it ranges beyond the three-year time-scale typical of the transition between stochastic and non stochastic processes (Kremlevskii et al. 1992; Lawrence et al. 1995). We recall that our rotation rate decreases by about 0.4% from cycle maximum to cycle minimum.

This north-south asymmetry is associated with an asymmetry in activity level with respect to the equator: the most active hemisphere is associated with faster and more rigid rotation. The northern hemisphere also exhibits a wider latitudinal range of activity: both sunspots and faculae extend 10° higher in latitude than in the southern hemisphere. North-south asymmetry in activity might be explained by the dynamo mechanism (for example by the superposition of a dipolar and a quadrupolar modes, see Sokoloff & Nesme-Ribes 1994). However, although a causal relationship of strong rotation asymmetry to strong activity asymmetry is straightforward, the reciprocal is less direct: the faster rotation of the more active hemisphere is not yet explained, nor is the faster rotation of young sunspots compared to plasma rotation. A number of attempts have been made to model the backreaction of the magnetic field on the velocity, and predict small amplitudes of the waves (Schüssler 1981; Yoshimura 1981), in disagreement with our observation of a strong north-south asymmetry.

Modeling of the north-south asymmetry is beyond the scope of the present paper. But it is of interest to mention the possible nonlinearities originating at the equator interface, since these play an important role. First, the dynamo waves of each hemisphere probably interact near the equator during the decreasing part of the cycle, and the two hemispheres are linked via the mainly dipolar poloidal field. Secondly, the presence of distinct meridional circulations near the equator suggests some interaction between the two hemispheres via diffusion processes. Such an interaction is also corroborated by the following observation: the average rotation rate of the folded hemispheres is close to the one observed for sunspots or magnetograms, which suggests an energy exchange between the two hemispheres. The kinetic energy associated with each hemisphere is 0.08% (North) and 0.03% (South) of the total kinetic energy of the layer showing this north-south asymmetry. Such an excess is not considerable if the phenomenon is restricted to shallow layers.

Lastly, we observed no torsional patterns when subtracting the cycle 19 mean rotation from the yearly data, as was done by previous authors. But the subtraction of the yearly polynomial fit from the corresponding yearly rotation rates averaged over latitude bins exhibits bands of faster and slower rotation rates with an amplitude of a few meters per second and a very small equatorward motion. The correspondence between this pattern and active regions is similar to that found by Snodgrass (1991) in the northern hemisphere. However, our pattern exhibits a strong north-south asymmetry that is not detected by Snodgrass.

Throughout this paper, we have stressed the differences between faculae and sunspots observed during the same period. Differences in anchorage depths and magnetic fields may provide explanations for this. This leads to important constraints on the dynamo model, especially the presence of a strong north-south asymmetry and its duration, and the shape-asymmetry of the rotation rates for both sunspots and faculae. The detection of a magnetic pattern similar to the oscillation patterns found by Snodgrass (1991) proves the validity of our method.

Acknowledgements. One of us (E. Nesme) is grateful to the Ministery of Defense, for having encouraged and funded the long-term spectroheliogram research program, through military contracts (no. 010481/ETCA, no. 012736/DRET-ETCA, and no. 92-2011.A/DRET-ETCA). The extensive work of the spectroheliogram observations team has been crucial for almost a century. We thank the present team for maintaining and improving the observational program over the years. Spectroheliograms were digitized with the *Machine à Mesurer pour l'Astronomie* (MAMA) of the Institut National des Sciences de l'Univers, at the Paris Observatory. Our thanks also go to P. Micheneau, R. Chesnel, P. Toupet, and M. Savinelli for their assistance in the data acquisition and processing. We used the Meudon *Cartes synoptiques de la chromosphère solaire et catalogue des filaments et des centres d'activité*.

References

Antonucci E., Hoeksema J.T. & Scherrer P.H., 1990, ApJ 360, 296
Belvedere G., Godoli G., Motta S., Paternò L. & Zappalà R.A., 1977, ApJ 214, L91
Collin B., Nesme-Ribes E., Leroy B., Meunier N. & Sokoloff D., 1995, C. R. Acad. Sci., Paris, t.321, Série IIb, 111
Howard R. & La Bonte B.J., 1980, ApJ 239, L33
Hoyng P., 1993, A&A 272, 321
Hoyng P., 1994, in: Solar Surface Magnetism, R.J. Rutten & C.J. Schrijver eds., 387
Komm R.W., Howard R.F. & Harvey J.W., 1993, Sol. Phys. 145, 1
Kremlevskii M.N., Blinov A.V. & Chervyakov T.B., 1992, Sov. Astron. Lett. 18(6), 423
Lawrence J.K., Cadavid A.C. & Ruzmaikin A.A., 1995, ApJ 455, 366
Mein P. & Ribes E., 1990, A&A 227, 577
Meunier N., Nesme-Ribes E. & Collin B., 1996, accepted in A&A (Paper II)
Maunder E.W. & Maunder A.S.D., 1905, M.N.R.A.S. 65, 813

Nesme-Ribes E., Ferreira E.N. & Mein P., 1993, A&A 274, 563
Nesme-Ribes E., Meunier N. & Collin B., 1996a, A&A 308, 213
Nesme-Ribes E., Meunier N & Vince I., 1996b, accepted in A&A
Newton H.W. & Nunn H.L., 1951, M.N.R.A.S. 111, 413
Press W.H., Flannery B.P., Teukolsky S.A. & Vetterling W.T., 1986, Numerical Recipes, Cambridge University Press
Roberts P.H., 1994, in: NATO ASI Series I, Vol. 25, E. Nesme-Ribes (ed.), 1
Schüssler M., 1981, A&A 94, L17
Snodgrass H.B., 1991, ApJ 383, L85
Sokoloff D.& Nesme-Ribes E., 1994, A&A 288, 293
Ternullo M., 1986, Sol. Phys. 105, 197
Vernazza J.E., Avrett E.H. & Loeser R., 1981, ApJ suppl. 45, 635
Ward F., 1966, ApJ 145, 416
Yoshimura H., 1981, ApJ 247, 1102

This article was processed by the author using Springer-Verlag LaTeX A&A style file *L-AA* version 3.